CHAPTER X COOKOFF REACTION VIOLENCE

Michael L. Hobbs[a*], Jonathan Baker[b], Malcolm D. Cook[c], Michael J. Kaneshige[a], Shane C. Schumacher[a], and Christopher Stennett[d]

[a]Sandia National Laboratories, Albuquerque NM USA; [b]AWE, Aldermaston, Reading, UK; [c]Syanco Ltd. West Malling, Kent UK; [d]Centre for Defence Chemistry, Cranfield University, Defence Academy of the UK, Shrivenham, Wiltshire, UK

*corresponding author, mlhobbs@sandia.gov

X INTRODUCTION

Cookoff refers to exposure of an explosive to an abnormally high temperature such as fire resulting in thermal ignition and a violent response with varying degrees of damage. Predicting when the explosive thermal ignites is a relatively straight forward problem if data is available, however, predicting the resulting violence is a major unsolved problem. The One-Dimensional-Thermal-Violence (ODTV) experiment was designed to provide quantitative violence response resulting from cookoff of explosives.

The ODTV experiment provides ignition time and wall velocity after 1 mm of lateral strain. We have determined that the wall velocity at this strain level correlates strongly with the number of fragments recovered after thermal ignition. In the current work, we present a model for both pre-ignition and post-ignition response of the ODTV experiment using an HMX-based explosive with a formulation of HMX/NC/K10 (91/1/8 by mass) with the most reactive components during pre-ignition being HMX (1,3,5,7-tetranitro-1,3,5,7-tetrazocane) and NC (nitrocellulose). A thermal model describes the spatial and temporal evolution of the energetic material up to ignition. Post ignition violence is evaluated following ignition.

X.1 Universal cookoff model and micromechanics pressurization model

Thermal ignition of the HMX-based explosives is modelled by solving the conductive energy equation in Table 1 that includes a volumetric source for three reactions that describe desorption of moisture, decomposition of HMX into equilibrium products, and decomposition of the nitrocellulose into equilibrium products. A modified Arrhenius rate is used to describe diffusion-limited moisture desorption and decomposition of the HMX and NC. Decomposition rates for the HMX and NC components are assumed to be autocatalytic.

Modified Arrhenius reaction rates are given in Table 1. Each reaction uses distributed activation energies with pressure dependent HMX and NC reaction rates. Autocatalysis is implemented via the distributed activation energy and pressure rather than concentrations. More information about this form of reaction rate has been published.[2] Latent effects for the β–δ phase change and HMX melting are accounted for using an effective capacitance method. Pressure is determined using a gas equation of state with an analytical expression for deformation of spherical defects caused by internal gas generation balanced by material strength of the confining explosive[3]. Details regarding this micromechanics pressurization model (MMP) can be found elsewhere[2]. The MMP parameters used for the HMX-based explosive include bulk modulus (1.14×10^{10} Pa), Young's modulus (9.56×10^{9} Pa), Poisson's ratio (0.36), distance between nucleation sites (0.000226 m), pore failure pressure (5×10^{6} Pa), and volumetric expansion coefficient (0.000131 K^{-1}).

The thermal model assumptions include 1) HMX and NC decompose into equilibrium products, 2) the conductive energy equation adequately describes volumetric energy sources from the chemical reactions, 3) energy transport is primarily by conduction rather than internal convection or radiation, 4) moisture evolves by diffusion-limited desorption rather than evaporation, 5) HMX and NC decomposition is autocatalytic where decomposition rates accelerate with respect to reaction extent by using a distributed activation energy, 6) reaction rates depend on confinement, 7) reaction rates are slower when the explosive is vented and faster when the explosive is sealed, 8) reaction rates are pressure-dependent using pressure build-up within the the explosive as well as the confinement, 9) the reaction rate accelerate by a factor of 10 as HMX melts between 529 and 531 K, 10) decomposition gases accumulate within defects or pockets within the explosive, 11) the defects change volume due to decomposition and mechanical strain caused by thermal expansion or compressibility, and 12) initially the explosive is impermeable to decomposition gases, but becomes permeable as the internal pore pressure exceeds 5 MPa.

80 Table X.1 *Thermal model with nomenclature/parameters in Table 2.*

Energy equation	$\rho C_p \frac{\partial T}{\partial t} = \nabla \cdot (k \nabla T) + h_{r1} r_1 + h_{r2} r_2 + h_{r3} r_3$	(1)
Mechanism (3 reactions)	$\mathrm{M} \xrightarrow{1} \mathrm{G}_M;\ \mathrm{H} \xrightarrow{2} 10\ G_H + 1.6\ \mathrm{C};\ \mathrm{N} \xrightarrow{3} 8.75\ G_N + 2.25\ \mathrm{C}$	(2)
Rate 1 (diffusion)	$r_1 = A_1 \exp\left(\frac{-E_1 + \zeta_1 \sigma_1}{RT}\right)[\mathrm{M}]$	(3)
Rate 2 (autocatalytic)	$r_2 = A_2 \left(\frac{P}{P_o}\right)^n \lambda T^m exp(-(E_2 + \xi_2 \sigma_2)/RT)[H]$	(4)
Rate 3 (autocatalytic)	$r_2 = A_3 \left(\frac{P}{P_o}\right)^n T^m exp(-(E_3 + \xi_3 \sigma_3)/RT)[N]$	(5)
Distribution function*	$\xi_1 = \mathrm{inv}([M]/[M]_o),\ \xi_2 = \mathrm{inv}([H]/[H]_o),\ \xi_3 = \mathrm{inv}([N]/[N]_o)$	(6)
Pressure	$P = z\rho RT/M_w$	(7)

81

82 Table 2. Nomenclature and model parameters

Symbols	Description	Value	Units
$\ln(A_1)$, $\ln(A_2)$, $\ln(A_3)$	Natural logarithm of the pre-exponential factors	35, 35, 35	$\ln(s^{-1})$
B	Binder	Binder is considered inert	None
[B]	Binder concentration	Constant: $(1-\omega_M)(\omega_B)\times\rho_{bo}/M_{wB}$ or 0.6826	kmol m^{-3}
C	Carbon	See Eq. (2)	None
[C]	Carbon concentration	Initially 0	Kmol m^{-3}
C_p	Specific heat[1] with linear interp. and constant extrap.	990 (300 K) 1188 (339 K) 1216 (349 K)	J kg^{-1} K^{-1}
E_1/R, E_2/R, E_3/R	Activation energy divided by *R*	25000, 15405, 15400	K
σ_1/R, σ_2/R, σ_3/R	Standard deviation of activation energy divided by R	2500, -1000, 500	K
G_H, G_M, G_N	HMX gas, desorbed moisture gas, and nitrocellulose gas	See Eq. (2)	None
$[G_H]$, $[G_M]$, $[G_N]$	Concentration of G_H, G_M, G_N	Initially 0	kmol m^{-3}
H	HMX	Used in Eq. (2) and as subscript	None
[H]	Conc. of HMX	Initially $(1-\omega_M)\times\rho_{bo}/M_{wH}$ or 5.5024	kmol m^{-3}
h_{fi} (i = M, G_M, H, G_H, C, N, G_N)	Heat for formation for i^{th} species	-285.8×10^6, -241.8×10^6, 75×10^6, -175×10^6, -650×10^6, -265×10^6	J $kmol^{-1}$
$h_{latent,\beta-\delta}$	Latent enthalpy for $\beta-\delta$ phase change	33000	J kg^{-1}
$h_{latent,m}$	Latent enthalpy for HMX melt	236000	J kg^{-1}
h_{ri} (i = 1, 2, 3)	Heat of reaction for i^{th} reaction (Hess's law)	$h_{r1} = (h_{fGm} - h_{fM}) = +44$ (endo) $h_{r2} = (10h_{fG} + 1.6h_{fC} - h_{fH}) = -1825$ (exo) $h_{r3} = (8.75h_{fG} + 2.25h_{fC} - h_{fN}) = -1670$ (exo)	J $kmol^{-1}$
i	i^{th} species or i^{th} reaction	M, G_M, H, G_H, C, N, G_N, 1, 2, 3	None
inv	Inverse of the standard normal distribution	Function (see Microsoft Excel NORMINV)	None
k	Thermal cond.[1] (linear interp. and constant extrap.)	0.31 (300 K), 0.37 (320 K)	W m^{-1} K^{-1}

λ	Rate acceleration factor for HMX melt.	Variable used to accelerate HMX decomposition rates when HMX melts. Transition occurs between 529 K and 531 K with λ changing from 1 to 10.	None
m	Steric factors	-2	None
[M]	Adsorbed moisture concentration	Initially $\omega_M \times \rho_{bo}/M_{wM}$ or 0.5	kmol m^{-3}
$[M_g]$	Desorbed moisture concentration	Initially 0	kmol m^{-3}
M_{wi} (i = M, G_M, H, G_H, C, N, G_N)	Molecular weight of i^{th} species	18, 18, 296.2, 27.6, 12, 297.1, 30.87	kg $kmol^{-1}$
N	Nitrocellulose	Used in Eq. (2) and as subscript	None
[N]	Concentration of N	Initially $(1-\omega_M)\times\rho_{bo}/M_{wN}$ or 0.0603	
n	Pressure exponent	0.49	None
P	Absolute pressure	Initially P_o	MPa
P_o	Initial pressure	0.083 (NM), 0.1 (CA and UK)	MPa
P_{fail}	Pore failure pressure	5	MPa
ρ	Density	Field variable	kg m^{-3}
ρ_{bo}	Initial bulk density	1800	kg m^{-3}
ρ_c	Condensed density	Field variable	kg m^{-3}
ρ_{co}	Initial condensed density	1841	kg m^{-3}
R	Gas constant	8314	m^3 Pa K^{-1} $kmol^{-1}$
[S]	Solid concentration	Initially 0	kmol/m^3
S_f	Solid fraction	$S_f = (Mw_M[\mathrm{M}] + Mw_W[\mathrm{W}] + Mw_S[\mathrm{S}] +)/\rho_{bo}$	kg kg^{-1}
t	Time	Global variable	s
T	Temperature	Field variable	K
[W]	Waste concentration	Initially $\omega_{waste}\times\rho_{bo}/M_{wW}$ or 4.07	kmol m^{-3}
T_o	Initial temperature	ODTV: 296 ODTX: 300 (guess) SITI: 297	K
V_{ex}	Extra gas volume (*i.e.*, expansion slot, pressure tube, etc)	ODTV: 4×10^{-6} ODTX: 0.07×10^{-6} SITI: 1.3×10^{-6}	m^3
V_o	Initial volume of explosive	ODTV: 14.1×10^{-6} ODTX: 1.1×10^{-6} SITI: 12.87×10^{-6}	m^3
ω_B	Initial mass fraction of inert binder	$(1-\omega_M)\times0.08 = 0.0796$	kg kg^{-1}
ω_H	Initial mass fraction of H	$(1-\omega_M)\times 0.91 = 0.90545$	kg kg^{-1}
ω_M	Initial mass fraction of adsorbed water	0.005	kg kg^{-1}
ω_N	Initial mass fraction of N	$(1-\omega_M)\times 0.01 = 0.00995$	kg kg^{-1}
ξ	inv: inverse of the standard normal distribution	Field variable	None
ξ_1, ξ_2, ξ_3	inv for 1st, 2nd, and 3rd reaction	Field variable	None
z	Gas compressibility	1 for ideal gas	None

X.2 Calibration of thermal model using SITI data

Sandia Instrumented Thermal Ignition (SITI) experiment (see Figure X.1) was used to determine the thermal conductivity and reaction parameters for the thermal model described in Table 1 using measured temperatures presented in Figure X.2.

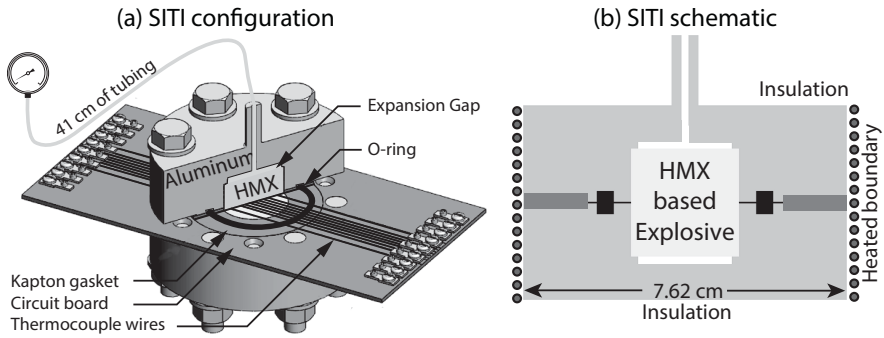

Figure X.1 SITI (a) configuration and (b) schematic.

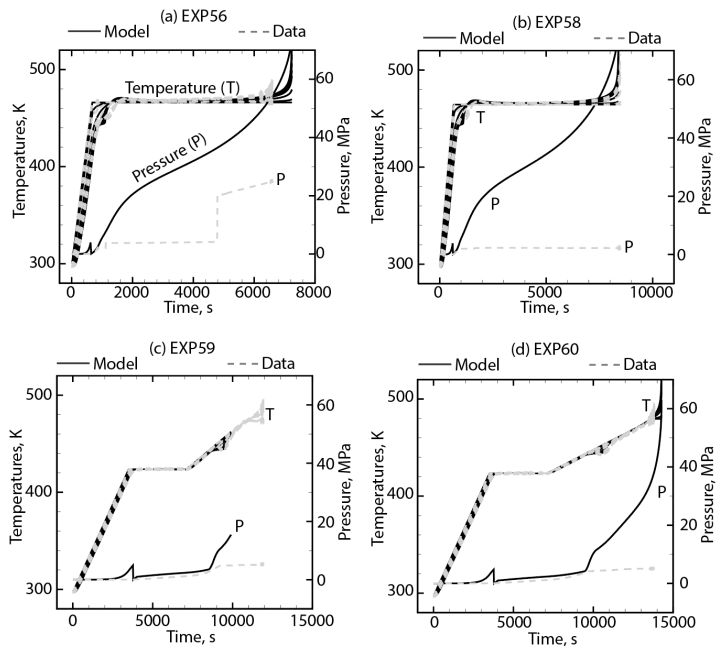

Figure X.2 SITI measured and predicted radial temperatures for SITI experiments with an average mass of 23.5 g and density of 1829 g/m^3.

The SITI experiment confines two 2.54 cm diameter by 1.27 cm tall cylinders of HMX-based explosive in aluminum with nine type K 127 μm (0.005 in.) diameter thermocouples located at radial positions in mm of 0, 1.70, 2.55, 3.40, 4.25, 5.11, 5.96, 8.81, and 11.7 and placed between the two explosive cylinders. The outer surface of the 7.62 cm diameter by 4.58 cm tall aluminum confinement is heated using rope heaters controlled by a thermocouple on the lateral surface (e.g., see Figure X.1a and Figure X.1b). Figure X.2 shows the external aluminum temperature measured for four SITI experiments. Two expansion gaps that are above and below the explosive are also machined into the confining aluminum. Each expansion gap has a diameter of 2.22 cm and is 0.16 cm tall.

Four SITI experiments were used to both parameterize and validate the reaction model: A) Exp56, B) Exp58, C) Exp59, and D) Exp60 with measured internal and boundary temperatures shown in Figure X.2 as dashed light gray lines. Exp56 was heated from 297 K to 466 K in 673 s and held until ignition. Exp58 was heated from 297 K to 464.33 K in 654 s and held until ignition. Exp59 was heated from 297 K to 423.75 K in 3500 s and held at 423.75 K until 7100 s, and then ramped to 473.34 K at 11930 s wherein the explosive thermally ignited. Exp60 was heated from 297 K to 423.35 K in 3500 s and held at 423.35 K until 7100 s, and then ramped to 479.36 K at 13826 s wherein the explosive thermally ignited. The predicted (solid black lines) and measured (dashed grey lines) radial temperatures and pressure are shown for each of the SITI experiments in Figure X.2

Exp58 in Figure X.2b was used to obtain the kinetic parameters for the model since this experiment clearly shows the β-δ phase change as well as a thermal excursion between 1000 and 2000 s. The other three SITI experiments (Exp56, Exp59, and Exp60) were used for validation. The measured and predicted (in parentheses with percent error) ignition times for these three experiments were 6603 s (7192 s, +9%), 11930 s (9926 s, -17%), and 12700 s (14200 s, +12%). These are reasonable predictions especially for high-density plastic bonded explosives that are at 98% of the theoretical maximum density (98%TMD). Lower density explosives are usually easier to predict since the decomposition gases are not retained within the explosive.

All SITI predictions were made assuming that the high-density HMX-based explosive was initially impermeable. A simple damage model was used to transition closed pores (impermeable) to open pores (permeable). The damage model determines when a pore fails, and thus allowing the pore gas to be part of the open pore network which includes the gases in the expansion gap. A maximum pore pressure of 5 MPa was chosen for the HMX-based explosive based on the work of others[2]. The predicted pressures show a spike when the internal pressures reach 5 MPa followed by a sudden decrease in pressure as the internal pressures are relieved as shown in the pressure predictions in Figure X.2. The measured pressures are from the pressure transducer that does not measure internal pressure build-up. In fact, the

simple pore damage model might not capture more complex damage that may result from heterogeneous cracking.

X.3 Validation of thermal model using ODTX and ODTV data

The schematics and ignition data for the one-dimensional time-to-explosion (ODTX) and the one-dimensional thermal violence (ODTV) experiments are shown in Figure X.3 and Figure X.4, respectively. The ODTX experiments[4] confine a 1.27 cm diameter sphere of explosive within two aluminum anvils that have hemispheres machined into each face. The maximum gas pressure within the ODTX confinement is 150 MPa. The explosive is sealed by plastically deforming a copper O-ring (shown in Figure X.3). Each aluminum anvil is held at the set point temperature (T_{sp}). At time zero, the hot anvils, heated and maintained at various set point temperatures, are brought together to hydraulically confine the initially room temperature explosive. The primary diagnostic for the ODTX experiment is the time required to reach thermal ignition.

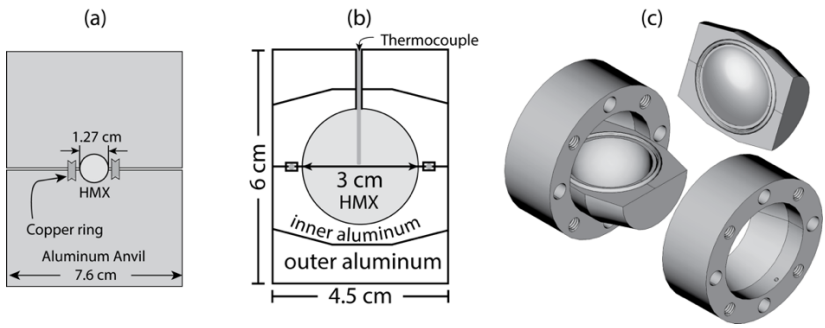

Figure X.3 (a) ODTX configuration, (b) ODTV schematic, (c) ODTV parts.

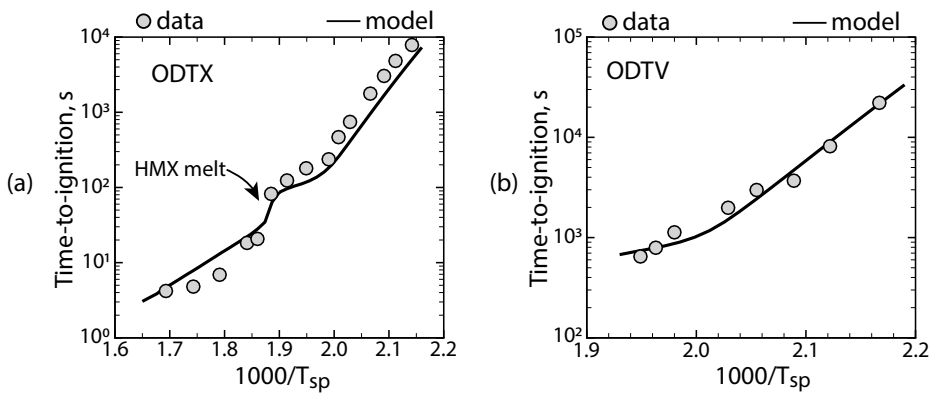

Figure X.4 Measured (symbol) and predicted (line) ignition data for the (a) ODTX experiments[4] and the (b) ODTV experiments[5].

The ODTV experiments[5] restrain a 3 cm diameter sphere of explosive using a double shell confinement (see Figure X.3b and X.3c). The confining aluminum is heated using induction heating. At time zero, the aluminum confinement is ramped from room temperature to the set point temperature in 300 s. The primary diagnostic for the ODTV experiment is ignition time, temperature measured in the center of the explosive, number of confinement fragments, and wall velocity using particle Doppler velocimetry (PDV). The maximum working pressure of the ODTV experiment was not measured and no limit on pressure was imposed on the ODTV model.

Predicted and measured time-to-ignition for both the ODTX and ODTV experiments for the HMX-based explosive are shown in Figure X.4. The parameters used to obtain the predictions in Figure X.4 were the same as used for the SITI predictions in Figure X.2. In the UCM/MMP model, the HMX reaction rate was increased by a factor of ten at the melting point to cause the distinct change in slope in the ignition plot as highlighted in Figure X.4(a).

The predicted temperature, pressure, and specific surface area for the ODTV experiment with the external temperature ramped from 296 K to 513 K in 300 seconds and then held until ignition is presented in Figure X.5. The temperature plot in Figure X.5(a) shows both the β–δ polymorphic phase transition as well as the melting of the HMX. The pressure plot in Figure X.5(b) shows the transition of the initially closed pore explosive (impermeable to gases) into an open pore explosive that is permeable to gases. The specific surface area shown in Figure X.5(c) was calculated with the MMP model and shows how thermal damage can be calculated for subsequent post ignition violence calculations. The ignition time for this simulation was 743 s. The measured ignition time was 648 s.

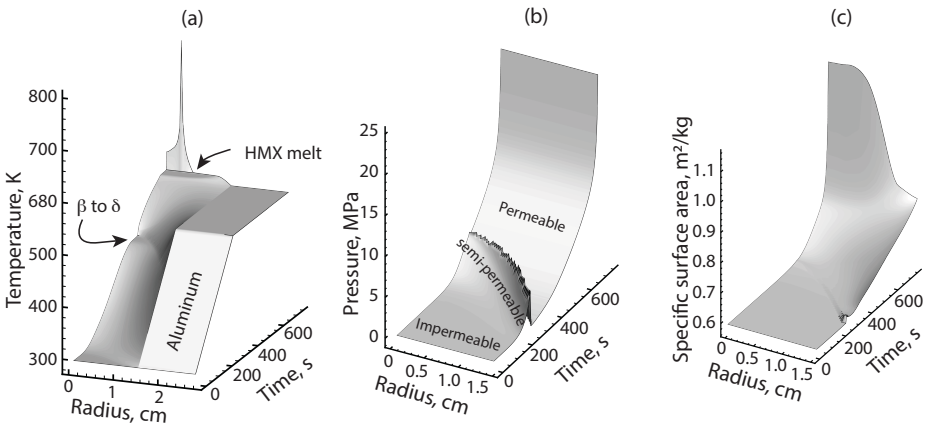

Figure X.5 Calculated (a) temperature, (b) pressure, and (c) specific surface area for the ODTV experiment with the external temperature ramped to 513 K.

X.4 Determining violence

Historically, violence is assessed post-mortem by counting the number of fragments. In all ODTV experiments shown in Figure X.4(b), the outer compression rings each produce 8 fragments for a total of 16 fragments regardless of the external heating rate. Damage occurs as the compression ring breaks at each of the 8 bolt holes. There are no bolt holes in the aluminum that surrounds the explosive, and the number of fragments originating from this confining aluminum defines the overall violence of the ODTV experiment. The number of inner confinement fragments, some of the measured velocities at a confinement displacement of 1.5 mm, and set point temperature for each of the eight ODTV experiments were 4 (240°C), 13 (237°C), 16 (232°C, 180 m/s), 24 (220°C), 21 (213°C, 140 m/s), 21 (205°C, 165 m/s), 31 (198°C, 210 m/s), and 38 (188°C, 205 m/s).

The simplest way to determine fragmentation of the confining aluminum in the ODTV experiment is by using a programmed burn following ignition. A program burn model assumes that the explosive burns at the detonation velocity starting at the location determined with the thermal ignition model which is typically near the center of the explosive (see Figure X.5a). In the current work, post-ignition calculations were performed by assuming the density of the explosive was either 1.8 g/cm^3 or 1.4 cm^3 with detonation velocities of 8.5 km/s and 7.2 km/s respectively. The product equation of state was determined using a JWL equation-of-state.

Predicted wall velocities using the two programmed burn models is shown in Figure X.6(a). The model used a two-dimensional axisymmetric mesh without bolt holes. A slide surface was used between the inner aluminum

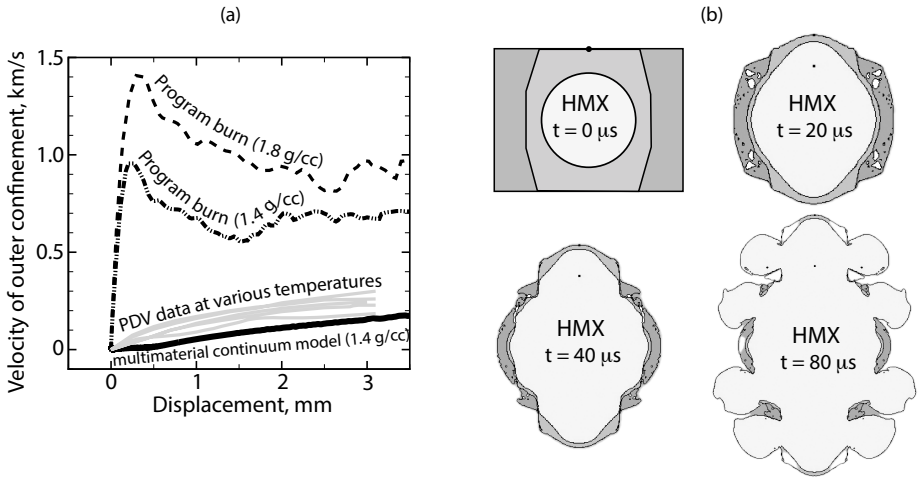

Figure X.6 (a) Predicted and measured confinement velocities and (b) material plots at various times for the programmed burn simulations at 1.8 g/cm^3.

confinement and the aluminum compression rings. For the aluminum, an elastic perfectly plastic von Mises (EPPVM) yield surface model with a yield strength of 945 MPa and a Poisson ratio of 0.3 were used in the simulations in Figure X.6. A simple Mie-Grüneisen equation of state with typical parameters was used for the aluminum equation-of-state. Fracture was assumed to occur when the aluminum was in tension at -900 MPa (negative sign indicates tension).

Figure X.6(b) shows sliding occurring between the inner confinement and compression rings and fragmentation of the aluminum for the higher density program burn calculation. Fragmentation of the confinement is usually determined by inserting void into computational cells when tension states exceed a critical level. The computed results are best near the onset of containment breakup. However, fragmentation cannot be accurately predicted without resolving the small aluminum grains which are on the order of microns in length. Such resolution is beyond the scope of the current paper.

The outer confinement velocities calculated with the simple programmed burn are much higher than the measurements shown in Figure X.6(a). Even the shape of the program burn velocities is incorrect. A better way to calculate the velocities is to use a multi-material continuum model for the HMX. Predictions from a multi-material model is also shown in Figure X.6(a) as well as Figure X.7(b) with magnitudes and shapes better approximating the measured velocity of the outer confinement. Material plots using the multi-material continuum model are shown in Figure X.7(a).

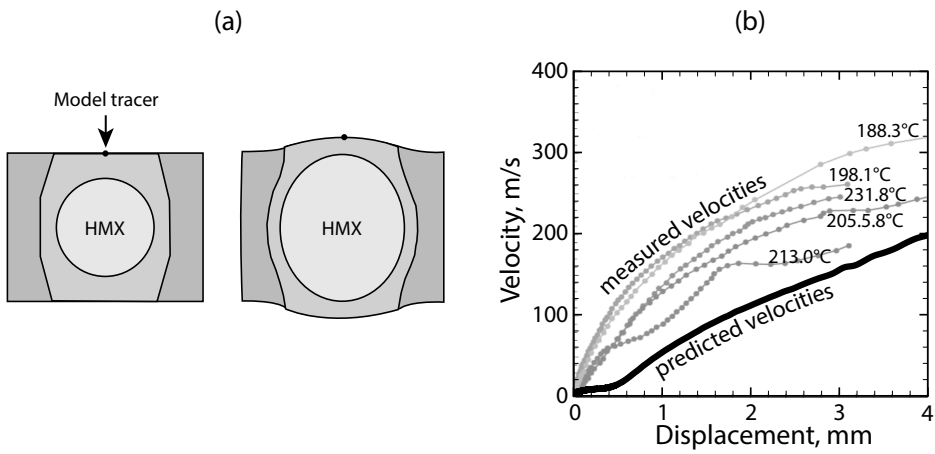

Figure X.7 (a) The ODTV experiment at two times following thermal ignition showing confinement deformation. (b) Measured (lines with symbols) and predicted (thick black line) of the outer confinement velocity at the tracer location shown in (a).

The velocity of the inner barrel-shaped containment was calculated using a generalized continuum mixture theory for the HMX-based material[7] implemented into a multi-material shock physics research code[8] using typical properties for the aluminum confinement. This code[8] can determine the behaviour of the explosive as it transitions from a subsonic deflagration to a supersonic detonation. Details regarding the multi-material mixture theory are beyond the scope of the present work and the interested reader is directed to the appropriate references[7,8]. The multi-material mixture model was initiated using a 1 mm bubble in the center of the explosive with a pressure and temperature (4370 MPa, 3540 K).

Unfortunately parameterizing the multi-material continuum model is complex and requires a substantial number of parameters and experiments at both pristine and heated conditions. However, parameters are available for a 1.4 g/cm^3 granular HMX[8] which is 74% of the theoretical maximum density (74%TMD). Parameters for the reactive constitutive model are not available for the higher density HMX-based explosive in the current work which is at 1.8 g/cm^3 (97%TMD). The predicted external velocity calculated with the multi-material mixture model using 1.4 g/cm^3 HMX is shown in Figure X.7.

The discrepancy between the measured and predicted velocities using the multi-material mixture model is primarily due to the lower density used in the model where the energy content in the model is crudely, 78% of the experiment. Another source of discrepancy is the delay in movement of the confinement that is absent in the data which shows immediate displacement of the outer surface. The model shows a delay in movement. Future work should enforce time synchronization between the experiments and the model.

Cook et al. [5], point out that the number of confining vessel fragments correlate to the measured velocity at a displacement of 1.5 mm. In the current work, fragmentation is correlated by using a simple model that assumes the fragmentation is dominated by fracture toughness[6]:

$$s = \left(\frac{\sqrt{24} K \left(1 - \frac{T}{T_m}\right)^n}{\rho c \dot{\varepsilon}} \right) \quad (8)$$

where s is a characteristic length of the fragment, K is the fracture toughness (20×10^6 Pa m$^{0.5}$), T is the ODTV set point temperature, T_m is the melting point of aluminum (933 K), n is the temperature exponent (-3.5), ρ is density of the aluminum (2700 kg m^3), C is the sound speed of the aluminum (3000 m/s), and $\dot{\varepsilon}$ is the strain rate. For the ODTV experiment, the strain rate can be approximated by either the measured or calculated confinement velocity normalized by the displacement at 1.5 mm.

Fragmentation is determined in the current work by using the damage model in Eq. (8), which require continuum strain predictions. The predicted velocities shown in Figure X.7(b) are not used to predict fragmentation due to lack of model parameters for the higher density HMX-based material

discussed in the current work. Instead, the velocity measurements are used with Eq. (8) to predict the number of fragments.

The measured velocity profiles shown in Figure X.7(b) are not distinctly different at small displacements. Once the displacement reaches about 1.5 mm, the velocity profiles have separated. The number of fragments is determined by calculating the characteristic dimension, S, from Eq. (8). The average fragment volume is then used with the ODTV aluminum volumes to determine the number of fragments.

$$\text{Number of fragments} = V_{\text{confinement}}/V_{\text{fragment}} \quad (9)$$

where V_{fragment} is the volume of the fragments calculated as s^3 and the volume of the inner confinement ($V_{\text{confinement}}$) is 34.5 cm^3. For reference, the volume of both compression rings is 67.6 cm^3 and the volume of the explosive is 14.1 cm^3. Other volumes include the O-ring space and the hole drilled for the internal thermocouple. Figure X.8 shows a comparison of the predicted and measured number of fragments.

Generally, the number of fragments decreases as the set point temperatures increase (see Figure X.8). However, there are several anomalies in both the predictions and measurements where the number of fragments increase with increasing temperature. For example, the model predicts an increase in the number of fragments at 232°C compared to 213°C.

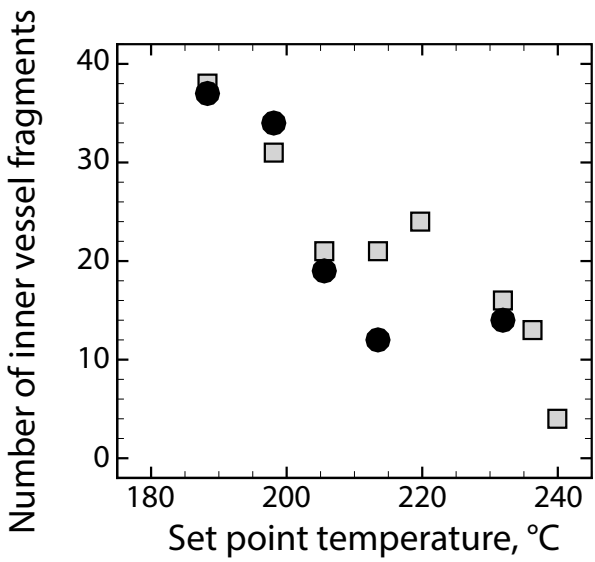

Figure X.8 Predicted (circles) and measured (squares) fragments of the barrel-shaped confinement vessel. There were 16 fragments from the compression rings.

This occurs since the model predictions are based on the measured wall velocity shown in Figure X.7(b) which show higher velocities for 232°C than for 213°C. The anomaly with the velocity at 232°C could have been caused by poor alignment of the PDV laser that was aimed too close to the joint at the mid-plane of the capsule. The PDV may have recorded the motion of several different surfaces during expansion[5].

Although the agreement between the predicted number and measured number of fragments is good, the agreement was obtained by judicious selection of the temperature exponent n (-3.5) in Eq. (8). To test this model, a future experiment should include powdered HMX at 1.4 g/cm^3.

X.5 Summary and conclusions

A universal cookoff model coupled to a micromechanics pressurization model (UCM/MMP) has been parameterized for an HMX-base explosive that also contains nitrocellulose. The model consists of three reactions that describe diffusion-limited moisture desorption, HMX decomposition, and nitrocellulose decomposition. The reaction rates use distributed activation energies. The HMX reactions were also increased by a factor of ten at the melting point. The UCM/MMP model was parameterized by using data from the Sandia Instrumented Thermal Ignition (SITI) experiment. The UCM/MMP model was validated using data from the one-dimensional time-to-explosion (ODTX) and one-dimensional thermal violence (ODTV) experiments without using any size dependent parameters.

A single post ignition example calculation for the ODTV experiment was performed using a continuum mixture model for a lower density HMX material. Predictions at the higher density were not attempted since model parameters were not available for the higher density material at elevated temperatures. Even though the predicted wall velocities were lower than the measured wall velocities, the predicted trends were similar.

Violence was calculated using a damage model that depends on the fracture toughness, set point temperature, melting temperature, density, sound speed, and strain rate. Strain rate was determined from the measured wall velocities. The predicted and measured number of fragments were similar. We recommend the ODTV experiments be run with pure HMX at density of 1.4 g/cm^3 to check the model. Parameterization of the multiple-material continuum model should also be done at the higher density and should include both pristine material and thermally-degraded material.

ACKNOWLEDGEMENTS

We would also like to thank Shane Snedigar for running the SITI experiments, Bill Erikson and Judith Brown for internal review, and Jeremy Lechman for management support. We would also like to thank AWE reviewers Rodney Drake and Caroline Handley. We would also like to thank AWE for supplying the material for the SITI experiments.

Sandia National Laboratories is a multimission laboratory managed and operated by National Technology & Engineering Solutions of Sandia, LLC, a wholly owned subsidiary of Honeywell International Inc., for the U.S. Department of Energy's National Nuclear Security Administration under contract DE-NA0003525. This paper describes objective technical results and analysis. Any subjective views or opinions that might be expressed in the paper do not necessarily represent the views of the U.S. Department of Energy or the United States Government.

X REFERENCES

1. Z. D. Lawless, M. L. Hobbs and M. J. Kaneshige, *Journal of Energetic Materials*, 2020, **38**, 214.

2. M. L. Hobbs, J. A. Brown, M. J. Kaneshige and C. Aviles-Ramos, *Propellants, Explosives, Pyrotechnics*, 2022, **47**, e202100155.

3. M. L. Hobbs, M. J. Kaneshige and W. W. Erikson, presented in part at 50th International Annual Conference of the Fraunhofer ICT, Karlsruhe, June, 2019.

4. C. M. Tarver and T. D. Tran, *Combustion and Flame*, 2004, **137**, 50.

5. M. D. Cook, C. Stennett and M. L. Hobbs, presented in part at the 16th International Detonation Symposium, Cambridge, July, 2018.

6. M. E. Kipp, D. E. Grady and J. W. Swegle, *International Journal of Impact* Engineering, 1993, **14**, 427.

7. M. R. Baer and J. W. Nunziato, *International Journal of Multiphase Flow,* 1986, **12**, 861.

8. S. C. Schumacher and M. R. Baer, *International Journal of Multiphase Flow,* 2021, **144**, 1.